The effect of micro- and macro-porosity of a titanium mesh for guided bone regeneration

Motoki Senoo

Nihon University Graduate School of Dentistry,

Major in Periodontology

(Directors: Prof. Shuichi Sato and Assist. Prof. Akira Hasuike)

Contents

The following article and new unpublished data (Fig. 6) are part of this doctoral thesis:

Motoki Senoo, Akira Hasuike, Takanobu Yamamoto, Yasumasa Ozawa, Norihisa Watanabe, Mitsuaki Furuhata, Shuichi Sato (2022) Comparison of macro-and micro-porosity of a titanium mesh for guided bone regeneration: An *In Vivo* experimental study. *In Vivo* 36, in press.

Abstract

Background/Aim: Guided bone regeneration (GBR) is one of surgical methods used for vertical ridge augmentation (VRA) prior to dental implant placements. Titanium meshes have been used for osteogenic space maintenance in GBR sites by clinicians. I aimed to compare the influence of micropores and macropores in a titanium mesh on bone regeneration in a rat calvarial vertical GBR model.

Materials and Methods: The calvaria of twelve rats was exposed, and plastic cylinders were set bilaterally. Twenty-four surgical sites were randomly allocated into four groups according to the materials of titanium lid and bone substitutes: microporous titanium lid + deproteinized bovine bone mineral (DBBM), macroporous titanium lid + DBBM, microporous titanium lid + carbonate apatite (CO_3AP), macroporous titanium lid + CO_3AP. Newly generated bone inside the cylinders was evaluated using micro-computed tomography (micro-CT). Furthermore, bone regeneration and angiogenesis were evaluated histologically at 12 weeks.

Results: Quantitative volumetric analyses using micro-CT showed a gradual increase in bone volume inside the cylinders in all four groups. Histological observation confirmed vigorous bone regeneration in the microporous groups compared to that in the macroporous group. In the upper part of the cylinders, soft tissue invaded the GBR site by passing through the pores of the macroporous mesh. The blood vessels in the upper part of the cylinders were smaller in the microporous groups than in the macroporous group. There was no difference in bone formation between cylinders filled with DBBM or carbonate apatite.

Conclusion: Microporous titanium mesh is a useful osteoconductive material for mechanical barrier in VRA, as it effectively supports angiogenesis from periosteum.

Introduction

The volumetric change in hard tissue dimensions is a critical consequence of tooth loss, which limits the optimal placement of dental implants. Many therapeutic modalities have been suggested to enhance the reconstruction of deficient alveolar ridges prior to implant placement [1]. Guided bone regeneration (GBR) is the most commonly used method for VRA; it enhances bone volume by guiding osteogenic cells to an area beyond the original skeletal envelope [2]. This surgical technique is based on the principle that mechanical barriers hinder epithelial and fibrous tissue invasion into the augmented bone. VRA is biologically demanding, as the influx of stem cells and blood flow needs to reach a certain distance from the existing bone for new bone formation. To explore these biological events, it is crucial to conduct *in vivo* assessments of GBR using preclinical models. A well-standardized rat GBR model with plastic cylinders placed on calvarial defects was developed [3-6].

GBR can be performed using several techniques, which are mainly based on the selection of bone substitutes and mechanical barriers. Several kinds of membranes have been used as mechanical barriers to prevent the invasion of fibrous tissue in regenerating bone defects. Conventionally, non-resorbable barrier membranes and resorbable barrier membrane have been used in clinical settings [7-10]. Although these commercially available membranes were reported to be highly predictable, they have several limitations. The first is their susceptibility to bacterial contamination. Second, membranes have a poor performance in terms of space maintenance, which is a fundamental prerequisite for any bone regeneration procedure. Unfortunately, the stiffness of membranes can be compromised by the pressure induced by the soft tissue inflammatory reaction and chewing process. To prevent the membranes from collapsing, the membrane should be thick so that the space for osseous regeneration becomes narrow.

The titanium products have been used to compensate for the limitations of these

conventional membranes [8, 9]. Titanium-reinforced polytetrafluoroethylene membranes are among the most documented membranes in VRA [11]. Although this material possesses characteristics such as biocompatibility, smoothness, and stiffness, the adaptation and fixation with bone pins or screws to the recipient site are technically demanding and time-consuming. Titanium meshes have also been used by clinicians for VRA since a long time [12]. According to current clinical reports, VRA with a titanium mesh has strong osteogenesis predictability, and most researchers achieved an average gain of 5-7 mm in bone height [13]. Titanium meshes in the dental market are macroporous, as the pore diameter is in the millimeter range. Since titanium mesh is far from occlusive, there is a possibility that fibrous tissue could intrude into the bone defect area and jeopardize bone regeneration. The influence of macroporosity remains controversial [6, 14, 15]. Several researchers have suggested that the pores of a titanium mesh play an essential role in establishing the supplement of osteogenic cells, growth factors, and blood supply from the periosteal overlying the barrier controversial [6, 14]. Hasegawa *et al*. developed a microporous titanium mesh with a pore diameter of 20 μm and a center-to-center distance of 50 μm [16]. The use of a laser processing system made it possible to create such tiny perforations at a high density. They reported strong osteogenesis predictability for internal GBR when this microporous titanium mesh was used with an autogenous iliac bone graft in a box-shaped ridge defect model of the dog mandible [17]. Recently, the first case was reported VRA with a microporous titanium mesh [18]. They showed successful results of simultaneous GBR with implant placement in the maxillary anterior region.

The present study aimed to compare the influence of micropores and macropores in titanium mesh used with bone substitutes on bone regeneration in a rat calvarial vertical GBR model. The dynamics of osteogenesis were elucidated by micro-computed tomography (micro-CT) and histological examination, and angiogenesis was also elucidated by histological examination.

Materials and Methods

Animals

This study was approved by the Animal Experimentation Committee of Nihon University School of Dentistry (AP18DEN027-1). Twenty-four surgical sites (250-300 g) of eight-week-old Fischer male rats were used in the experiments. The primary outcome was percentage of newly formed bone in histology. The sample size was calculated with G*Power software v. 3.1(University of Dusseldorf, Dusseldorf, Germany) using Wilcoxon-Mann-Whitney test at an alpha level of 0.05 and a statistical power of 95% based on the previous study [6], in which percentage of newly formed bone from occlusive and non-occlusive barriers showed significant statistical difference between 25 ± 3% and 17 ± 3%. All animals were housed in cages to ensure standardized environmental factors during the experimental period.

Surgical Procedures

The standardized rat calvarial vertical GBR model developed by the present group was used [3-6]. Before the surgical session, the animals were anesthetized via initial inhalation of 4% (v/v) isoflurane for 2 minutes, followed by intraperitoneal injection of a mixture of 0.15 mg/kg dexmedetomidine hydrochloride, 2.0 mg/kg midazolam, and 2.5 mg/kg butorphanol tartrate. A 0.5 ml solution of 1: 80,000 dilution of lidocaine (Xylocaine; Astra Zeneca, Osaka, Japan) was administered locally to control bleeding and pain. After shaving and disinfecting with 70% ethanol swabs in the region between the eyes and the posterior end of the skull, a midline incision of 6.0 cm was made, and a mucoperiosteal flap was elevated with a small sharp periosteal elevator to expose the cranial vertex. Two standardized circular grooves of 5mm diameter were made at the center of each parietal bone using a trephine bur with an external diameter and a trephine drill. The trephine burr was used under constant irrigation with 0.9% saline to prepare the grooves without damaging the inner dura of the cranial bone. To induce bleeding, five small penetration holes were drilled with a small round burr (Fig. 1A).

After exhaustively washing the surgical area with sterile saline to remove any bone scraps, plastic cylinders (5.0 mm diameter, 3.0 mm height) were pressed into the circular grooves (Fig 1B). The plastic cylinders were filled with bone substitutes and covered with titanium lids. Using a computer-generated random sequence, twenty-four surgical sites were randomly allocated into four groups according to the titanium lid and bone substitute materials.

1. Microporous titanium lid (Ti honeycomb membrane, Morita, Tokyo, Japan) (Fig 2A, B) + deproteinized bovine bone mineral (DBBM, Bio-Oss®, Geistlich-Pharma, Wolhusen, Switzerland): MicroTi+ DBBM

2. Macroporous titanium lid (titanium mesh, Jeil Medical, Seoul, South Korea) (Fig. 2C, D) + DBBM: MacroTi + DBBM

3. Microporous titanium lid (Fig. 2A, B) + carbonate apatite (CO_3AP, Cytrans®, GC, Tokyo, Japan): MicroTi + CO_3AP.

4. Macroporous titanium lid + CO_3AP: MacroTi + CO_3AP.

After surgery, the skin and periosteum were repositioned and sutured with simple resorbable interrupted sutures (VSORB 4-0, Washiesu Medical, Tokyo, Japan). The day of surgery was designated as day 0. All rats were euthanized 12 weeks post-surgery.

Micro CT analysis

The total volumes of the minerals at the surgical sites in MicroTi+ DBBM, MacroTi + DBBM, and MicroTi + CO_3AP were evaluated repeatedly by radiography. An *in vivo* micro-CT system (R_mCT2 system; Rigaku, Tokyo, Japan) was used for imaging at 0, 4, 8, and 12 weeks postoperatively without euthanasia. The rats were seated on an imaging stage and anesthetized by inhalation of an oxygen-isoflurane mixture via a facemask. The exposure parameters were 90 kV and 100 μA. The region of interest (ROI) for micro-CT assessment was defined as the circular grooves made on the calvaria, each of which had a diameter of 5.0 mm and a height of 3.0 mm. Images were reconstructed on a personal computer using the i-View

software (i-View Image Center, Tokyo, Japan). The bone volume within the plastic caps in the voxel images was examined using the same software. The enhanced volume was calculated by subtracting the volume on day 0 from the values obtained from each follow-up. Measurements were taken by one experienced and blinded examiner for micro-CT assessment.

acid.

Histological analysis

Histomorphometric analyses of histological sections, osteogenesis, and angiogenesis at the experimental GBR sites in MicroTi + DBBM, MacroTi + DBBM, MicroTi + CO_3AP and MacroTi + CO_3AP were conducted. All rats were euthanized by excess CO_2 gas inhalation at 12 weeks postoperatively. The bone segments containing the cylinders were resected from the surgical sites and fixed in 10% neutral-buffered formalin, and then decalcified with 5 % formic decalcified. The decalcified samples were dehydrated with graded ethanol, defatted in xylene, and embedded in paraffin wax blocks. Blocks were processed into 5-μm sections at the central region of the cylinder and stained with Masson's trichrome staining to detect collagen and lamellar bone formation. Histomorphometric assessments of the sections were conducted under a light microscope and an image analyzer computer system using ImageJ software (National Institutes of Health, Maryland, USA). The total ROI for histomorphometric analysis was divided into three parts: ROI1 referred to the region that covered 1.0 mm of the defect closest to the calvaria, ROI3 referred to the upper 1.0 mm of the defect, and ROI2 referred to the central region between ROI1 and ROI3. (Fig. 3)

The following variables were assessed:

・Percentage of newly formed bone in total ROI: Area of newly formed mineralized bone tissue (mm^2) / area of total ROI (mm^2).

・Percentage of residual granules in the total ROI: area of residual granules (mm^2) / area of total ROI (mm^2).

・Number of blood vessels in each ROI: Vessels were quantified after scanning the section at 10 × magnification. For the selection of vessels, only those showing lumens were quantified.

・Blood vessel size in each RIO: area of blood vessels (mm^2) / number of blood vessels in each ROI.

Measurements were taken by one experienced and blinded examiner for histomorphometric assessment.

Statistical analysis

In micro-CT assessment, means and standard deviations (SD) of the bone volume within the plastic caps were collected. In histological analysis, the median, percentiles, and maximum and minimum values of each variable were displayed. Data were analyzed for statistical significance using a Kruskal-Wallis test with a Steel-Dwass post hoc test. All variables were analyzed using EZR (Saitama Medical Center, Jichi Medical University, Saitama, Japan), a graphical user interface for R 2.13.0, (R Foundation for Statistical Computing, Vienna, Austria). $p<0.05$, were considered statistically significant.

Results

No surgical complications occurred during the cylinder placement. All animals healed normally, with no postoperative complications such as pain, fever, or infection.

Micro CT analysis

Micro-CT images of representative surgical sites in each group are shown (Fig. 4). Although the pores of the macroporous titanium lid were confirmed by sagittal CT sections, the pores of the microporous titanium lid were not. Micro-CT images showed that the radiopaque contrast increased gradually inside the cylinders of all three groups. In the sagittal images of all three groups at 12 weeks, the gap between particles was partially filled with radiopacity. At all observational periods, the profile of each DBBM particle was confirmed clearly, in contrast to that of CO_3AP, which was shown as a mass of several particles. At 12 weeks, partial reossification images inside five small penetration holes were confirmed in all three groups. Quantitative volumetric analyses showed a gradual increase in the bone volume inside the cylinders in all three groups. The differences between the three groups were not statistically significant (Table 1).

Histological analysis

Representative histological specimens stained with Masson’s trichrome stain are shown (Fig. 5). The regenerated bone presented with a mature mineralized trabecular appearance. Osteoid borders on the bone surface indicate active osteogenesis. Soft tissue invasion was observed in all groups, and the most prominent growth of invasive soft tissue was observed in cylinders covered with macroporous titanium mesh. High magnification images of the area with soft tissue invasion, residual particle, and the newly formed bone tissue are presented (Figs. 5B, D, and F). Smaller blood vessels were seen in cylinders covered with microporous titanium lids compared to that seen in cylinders with macroporous titanium lids. Histological sections of MacroTi + CO_3AP stained with Masson's Trichrome is shown (Fig. 6). As with

Macro Ti + DBBM group, soft tissue invasion through macro pores was confirmed. Newley generated bone surrounded aggregated particles, and the regenerated bone showed mature mineralization.

The results of the quantitative analysis of histology are shown as box plots (Figs.7, 8). The percentage of newly formed bone tissue in cylinders covered with microporous titanium lids was significantly higher than that in cylinders with macroporous titanium lids (MicroTi + DBBM: 40.0 ± 4.5%, MicroTi + CO_3AP: 37.8 ± 3.6%, Macro Ti + DBBM: 31.5 ± 4.7%) (Fig. 7A). At 12 weeks, more than one-third of the bone substitute particles remained unabsorbed in all three groups (MicroTi + DBBM: 35.7 ± 3.2%, Macro Ti + DBBM: 35.8 ± 3.7%, MicroTi + CO_3AP: 34.0 ± 3.8%) (Figure 7B). In the lower third of the ROI (ROI1), the numbers of blood vessels was smaller in the microporous titanium groups than in the macroporous titanium group (MicroTi + DBBM: 17.3 ± 2.4, Macro Ti + DBBM: 27.5 ± 4.8, MicroTi CO_3AP: 19.0 ± 4.6) (Fig. 8A). In the upper third of the ROI (ROI3), there was no significant difference in the number of blood vessels between the three groups (MicroTi + DBBM: 22.5 ± 5.2, Macro Ti + DBBM: 27.3 ± 4.2, MicroTi + CO_3AP: 23.0 ± 4.2) (Fig. 8A). In the analysis of blood vessel size in the upper third of ROI, blood vessels were smaller in the microporous titanium groups than in the macroporous titanium group (MicroTi + DBBM: 2.9 ± 0.7 × 10^{-3} mm^2, Macro Ti + DBBM: 6.2 ± 0.9 × 10^{-3} mm^2, MicroTi + CO_3AP: 2.8 ± 1.7 × 10^{-3} mm^2) (Fig. 8B).

Discussion

This study compared the influence of microporous titanium on the vertical GBR. Histological observation confirmed more vigorous bone regeneration in the microporous groups than in the macroporous group. In the upper part of the GBR sites, microporous titanium meshes prevented invasion of soft tissue, and enabled microangiogenesis. The data showed superiority of microporous titanium in angiogenesis and ample blood supply, which play a critical role in promoting bone regeneration. A pore diameter in the micrometer range is more suitable for bone regeneration compared to a pore diameter in the millimeter range.

Wang *et al*. described four major biological requirements for predictable GBR: primary wound closure, angiogenesis, space maintenance, and stability [19]. During GBR surgery, the addition of bone substitutes and mechanical barriers plays a major role in space maintenance. In the healing phase following GBR surgery, the growth of new blood vessels inside the secured space is one of the most important factors for successful GBR. The initial healing step is characterized by the formation of a blood clot. This is followed by the replacement of the blood clot with granulation tissue. Blood vessels are bound to the granulation tissue and are key to the osteoid formation of woven bone. An intimate relationship exists between newly formed blood vessels and *de novo* bone formation. Blood supply from the marrow is a rich source of growth factors and undifferentiated cells [20].

The periosteal covering the barrier could be another candidate for the origin of blood supply. Considering angiogenesis from the periosteal, the permeability of mechanical barriers is required. The previous study compared several sizes of macropores in rat calvarial models that were similar to those used in the present study [6]. The pore size created at the lid of the barrier was identical to that of the pores used in commercially available titanium meshes. As a result, barrier permeability in meshes with pores in the millimeter range resulted in less augmented bone, compared with the occlusive barrier. This could be attributed to the fact that fibrous tissue

ingrowth occurred from the outside by passing through the millimeter-range pores. The histological results obtained from the macroporous group in the present study correspond with this result. However, the microporous groups showed fibrous tissue volume in the upper part of the cylinders and an abundant volume of newly formed woven bone. In the upper part of the GBR sites just beneath the periosteal tissue, sufficient microvasculature was also observed in the microporous groups. Thus, it could be concluded that micrometer-range pores enabled microangiogenesis and prevent soft tissue ingrowth.

In the present study, two types of particulate bone grafts were placed inside the cylinders covered with macro Ti or micro Ti. DBBM is a widely utilized bone graft material, especially in countries where the use of allografts is not permitted. Although xenografts were first developed to act as a standard replacement material similar to autografts and allografts, xenografts typically do not resorb over time. A CO_3AP bone substitute was recently developed as an alternative to allografts and xenografts [21]. Commercially available CO_3AP particles are chemically pure; they are manufactured by a dissolution-precipitation reaction in aqueous solution using a calcite block, rather than through a sintering process. In a previous study on rabbit femurs, at 8 weeks, faster bone formation was observed in defects filled with CO_3AP than in those filled with DBBM [22]. The present study also showed the bone regenerative capacity of CO_3AP, which is comparable to that of DBBM. Furthermore, both materials remained almost 30% unabsorbed at 12 weeks. Thus, these bone substitutes can be categorized as unabsorbable osteoconductive materials. Differences in particle appearance between these two bone substitutes were confirmed by micro-CT and histological analysis. At 4 weeks, micro-CT confirmed particle aggregation of CO_3AP particles. Whereas, DBBM particles were scattered inside the cylinders. In histological sections at 12 weeks, bone formation was confirmed around the aggregated particles of CO_3AP, as well as surrounding the scattered particles of DBBM. The difference in particle appearance may influence the quality of newly

formed bone.

The major limitation of present work was only focused on the permeability of two different titanium mesh. The size of the pores is not the only relevant factor for titanium mesh in osteogenesis. These two products have several differences in their properties, such as thickness, smoothness, and toughness. These properties may be confounding factors in bone regeneration. In future studies, the use of identical titanium meshes (except for their permeability) is ideal for further assessment. In addition, the collaborative effect of microporosity and surface structure also needs to be examined [23].

Conclusion

Microporous titanium mesh is a useful osteoconductive material for mechanical barrier in VRA, as it effectively supports angiogenesis from periosteum.

Acknowledgements

This work was financially supported by the Dental Research Center, Nihon University School of Dentistry. This work was also financially supported by JSPS KAKENHI grants JP19K19061 (Grant-in-Aid for Young Scientists) and JP17K11810 (Grant-in-Aid for Scientific Research (C)).

References

1. Plonka A, Urban I, Wang H-L (2018) Decision tree for vertical ridge augmentation. Int J Periodontics Restorative Dent 38, 269-275.
2. Dahlin C, Linde A, Gottlow J, Nyman S (1988) Healing of bone defects by guided tissue regeneration. Plast Reconstr Surg 81, 672-676.
3. Kochi G, Sato S, Fukuyama T, Morita C, Honda K, Arai Y, Ito K (2009) Analysis on the guided bone augmentation in the rat calvarium using a microfocus computerized tomography analysis. Oral Surg Oral Med Oral Pathol Oral Radiol Endod 107, e42-48.
4. Oginuma T, Sato S, Udagawa A, Saito Y, Arai Y, Ito K (2012) Autogenous bone with or without hydroxyapatite bone substitute augmentation in rat calvarium within a plastic cap. Oral Surg Oral Med Oral Pathol Oral Radiol 114, S107-113.
5. Kubota T, Hasuike A, Naito M, Tsunori K, Min S. Sato S (2018) Enhancement of bone augmentation in osteoporotic conditions by the intermittent parathyroid hormone: an animal study in the calvarium of ovariectomized rat. Int J Oral Maxillofac Implants 33, 1003-1010.
6. Yamamoto T, Hasuike A, Koshi R, Ozawa Y, Ozaki M, Kubota T, Sato S (2018) Influences of mechanical barrier permeability on guided bone augmentation in the rat calvarium. J Oral Sci 60, 453-459.
7. Simion M, Fontana F, Rasperini G, Maiorana C (2007) Vertical ridge augmentation by expanded-polytetrafluoroethylene membrane and a combination of intraoral autogenous bone graft and deproteinized anorganic bovine bone (Bio Oss). Clin Oral Implants Res 18, 620-629.
8. Hämmerle CHF, Jung RE, Yaman D, Lang NP (2008) Ridge augmentation by applying bioresorbable membranes and deproteinized bovine bone mineral: a report of twelve consecutive cases. Clin Oral Implants Res 19, 19-25.

9. Soldatos NK, Stylianou P, Koidou P, Angelov N, Yukna R, Romanos GE (2017) Limitations and options using resorbable versus nonresorbable membranes for successful guided bone regeneration. Quintessence Int 48, 131-147.
10. Urban IA, Montero E, Monje A, Sanz-Sánchez I (2019) Effectiveness of vertical ridge augmentation interventions: A systematic review and meta-analysis. J Clin Periodontol 46 Suppl. 21, 319-339.
11. Urban IA, Lozada JL, Jovanovic SA, Nagursky H, Nagy K (2014) Vertical ridge augmentation with titanium-reinforced, dense-PTFE membranes and a combination of particulated autogenous bone and anorganic bovine bone-derived mineral: a prospective case series in 19 patients. Int J Oral Maxillofac Implants 29,185-193.
12. von Arx T, Hardt N, Wallkamm B (1996) The TIME technique: a new method for localized alveolar ridge augmentation prior to placement of dental implants. Int J Oral Maxillofac Implants 11, 387-394.
13. Xie Y, Li S, Zhang T, Wang C, Cai X (2020) Titanium mesh for bone augmentation in oral implantology : current application and progress. Int J Oral Sci 12, 37.
14. Ikeno M, Hibi H, Kinoshita K, Hattori H, Ueda M (2013) Effects of the permeability of shields with autologous bone grafts on bone augmentation. Int J Oral Maxillofac Implants 28, e386-392.
15. Jang YS, Moon SH, Nguyen TDT, Lee MH, Oh TJ, Han AL, Bae T (2019) In vivo bone regeneration by differently designed titanium membrane with or without surface treatment: a study in rat calvarial defects. J Tissue Eng 10, 2041731419831466.
16. Hasegawa H, Masui S, Ishihata H (2018) New microperforated pure titanium membrane created by laser processing for guided regeneration of bone. Br J Oral Maxillofac Surg 56, 642-643.
17. Hasegawa H, Masui S, Ishihata H, Kaneko T, Ishida D, Endo M, Kanno C, Yamazaki M,

Kitabatake T, Utsunomiya S, Izumi K, Sasaki K (2019) Evaluation of a newly designed microperforated pure titanium membrane for guided bone regeneration. Int J Oral Maxillofac Implants 34, 411-422.

18. Ishikawa T, Ueno D (2020) Vertical ridge augmentation with a honeycomb structure titanium membrane: A technical note for three-dimensional curvature bending method. J Oral Implantol 47, 411-419.
19. Wang HL, Boyapati L (2006) “PASS” principles for predictable bone regeneration. Implant Dent 15, 8-17.
20. Min S, Sato S, Murai M, Okuno K, Fujisaki Y, Yamada Y, Ito K (2007) Effects of marrow penetration on bone augmentation within a titanium cap in rabbit calvarium. J Periodontol 78, 1978-1984.
21. Ishikawa K (2010) Bone substitute fabrication based on dissolution-precipitation reactions. Materials (Basel) 3, 1138-1155.
22. Fujisawa K, Akita K, Fukuda N, Kamada K, Kudoh T, Ohe G, Mano T, Tsuru K, Ishikawa K, Miyamoto Y (2018) Compositional and histological comparison of carbonate apatite fabricated by dissolution-precipitation reaction and Bio-Oss®. J Mater Sci Mater Med 29, 121.
23. Hartjen P, Hoffmann A, Henningsen A, Barbeck M, Kopp A, Kluwe L, Precht C, Quatela O, Gaudin R, Heiland M, Friedrich RE, Knipfer C, Grubeanu D, Smeets R, Jung O (2018) Plasma electrolytic oxidation of titanium implant surfaces: Microgroove-structures improve cellular adhesion and viability. In Vivo 32, 241-247.

Figures

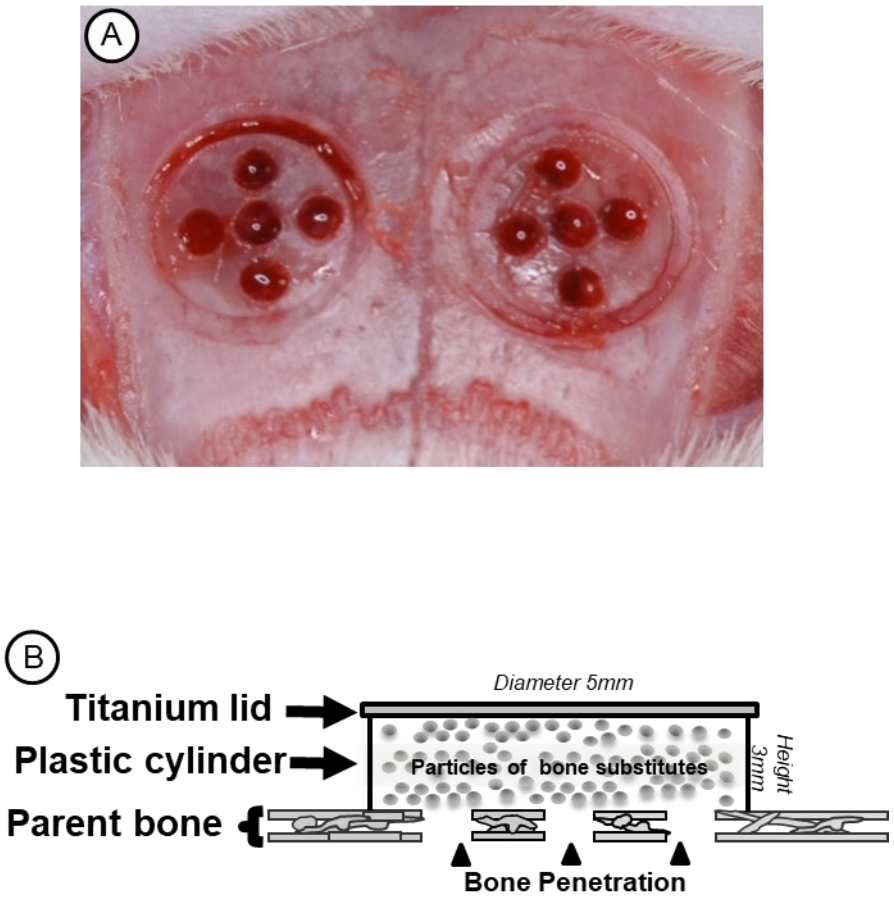

Fig. 1 A circular groove was made with a trephine bur, and five small holes were drilled with a round bur to allow for marrow penetration (A); A schematic depiction of the rat experimental model (B).

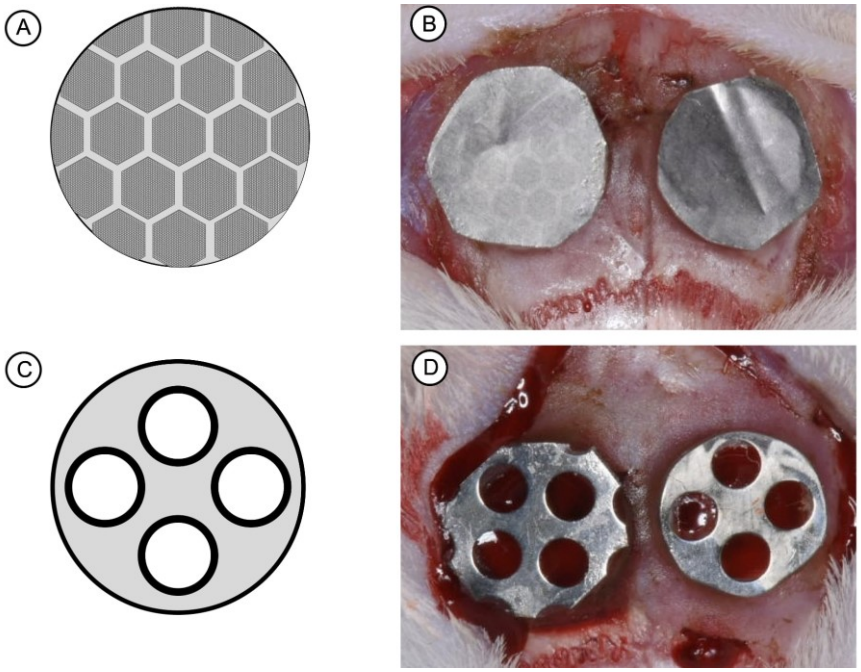

Fig. 2 A schematic depiction of microporous titanium lids (A); cylinders with microporous titanium lids were set on the both sides of calvaria (B); a schematic depiction of macroporous titanium lids (C); cylinders with macroporous titanium lids were set on both sides of calvaria (D).

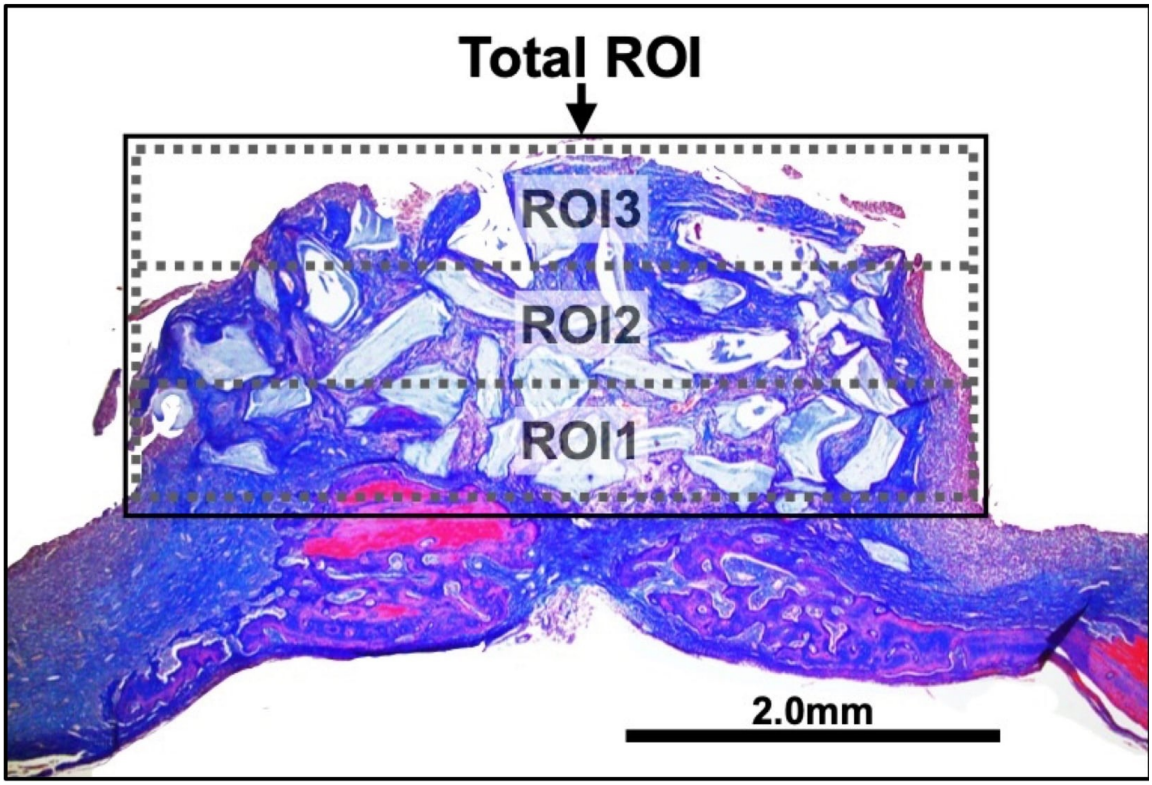

Fig. 3 Image representing regions of interest (ROI) in histological assessment.

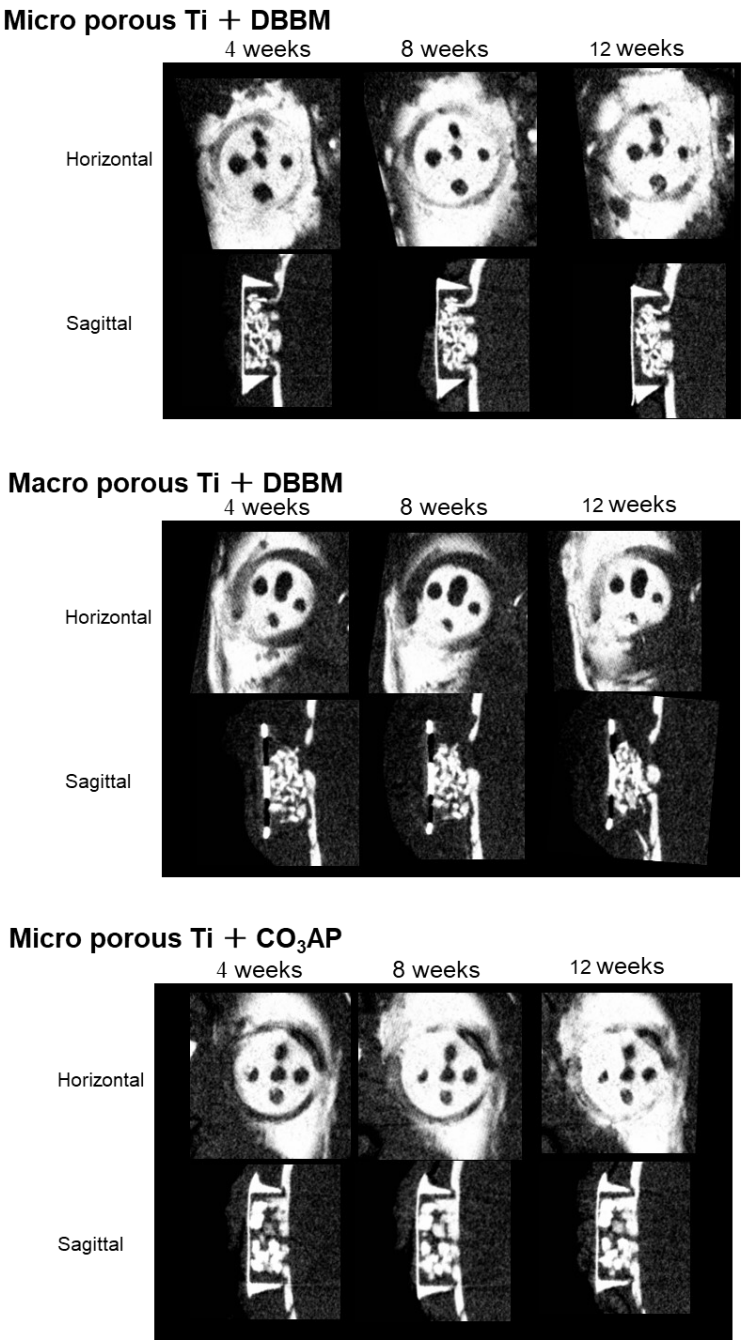

Fig. 4 Micro-computed tomography analysis was performed.

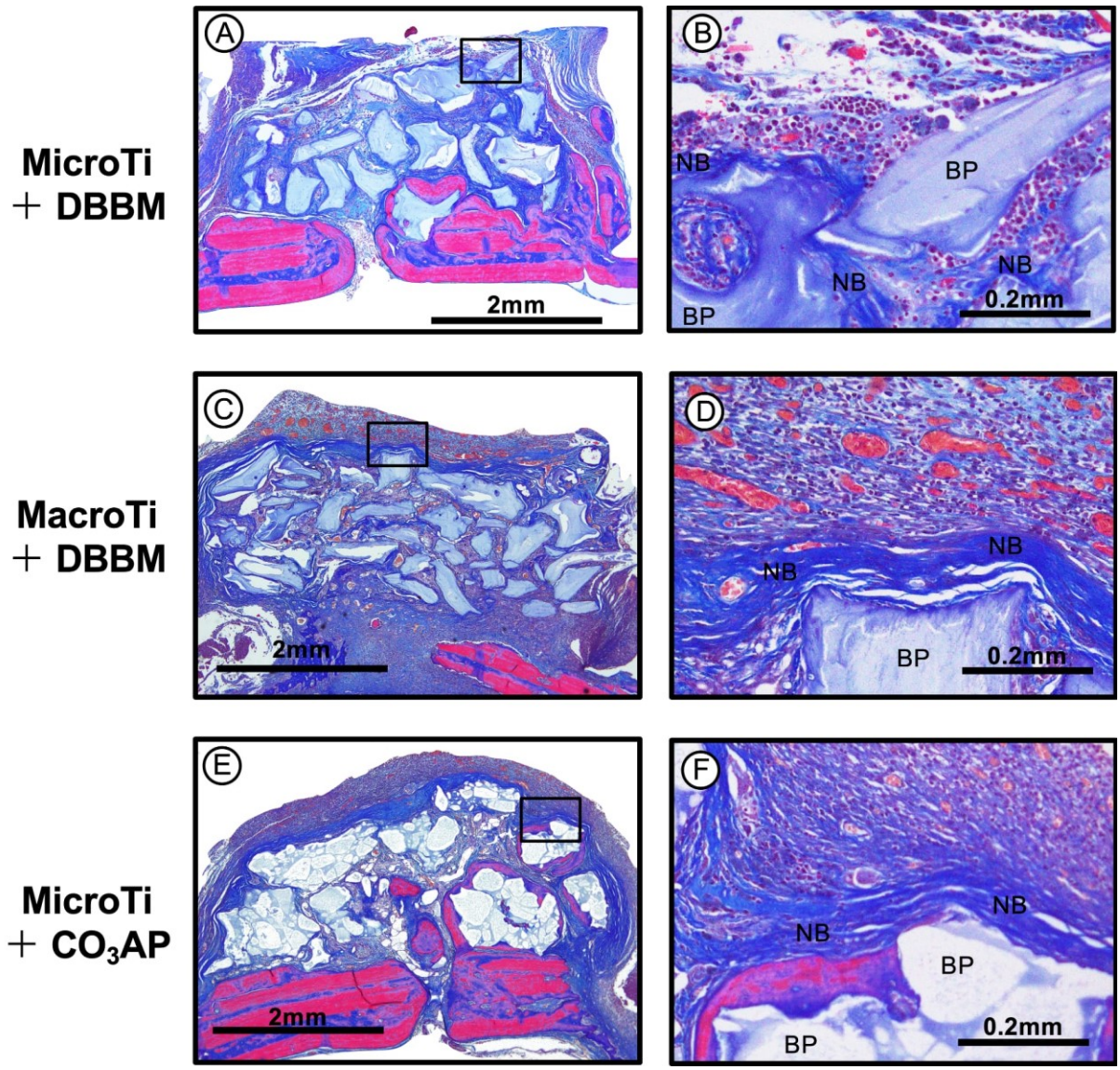

Fig. 5 Representative histological specimens of each group at 12 week stained with Masson trichrome. Lower magnification (A)(C)(E); Higher magnification (B)(D)(F). NB = new bone; BP: Biomaterial particle.

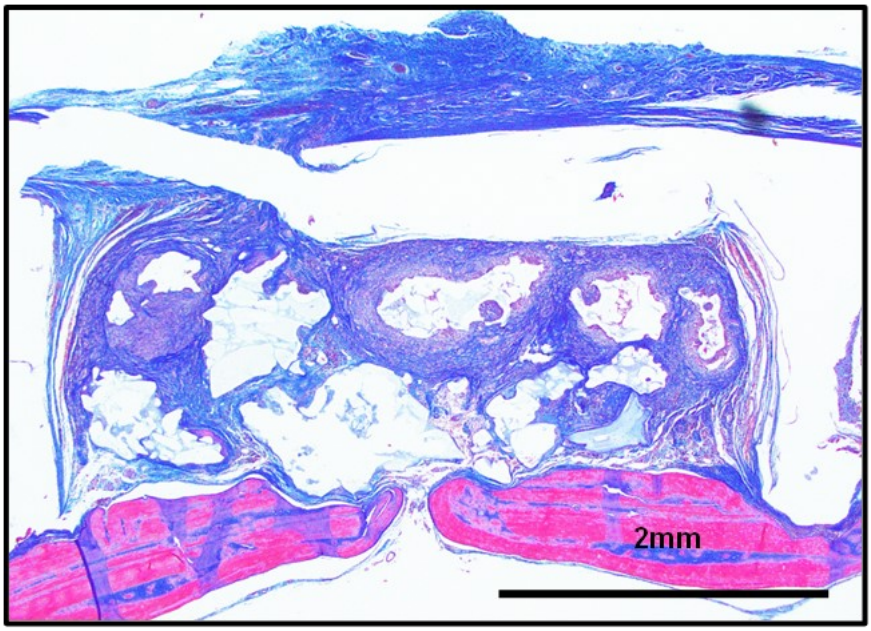

Fig. 6 Representative histological specimens of MacroTi + CO_3AP group at 12 week stained with Masson's trichrome.

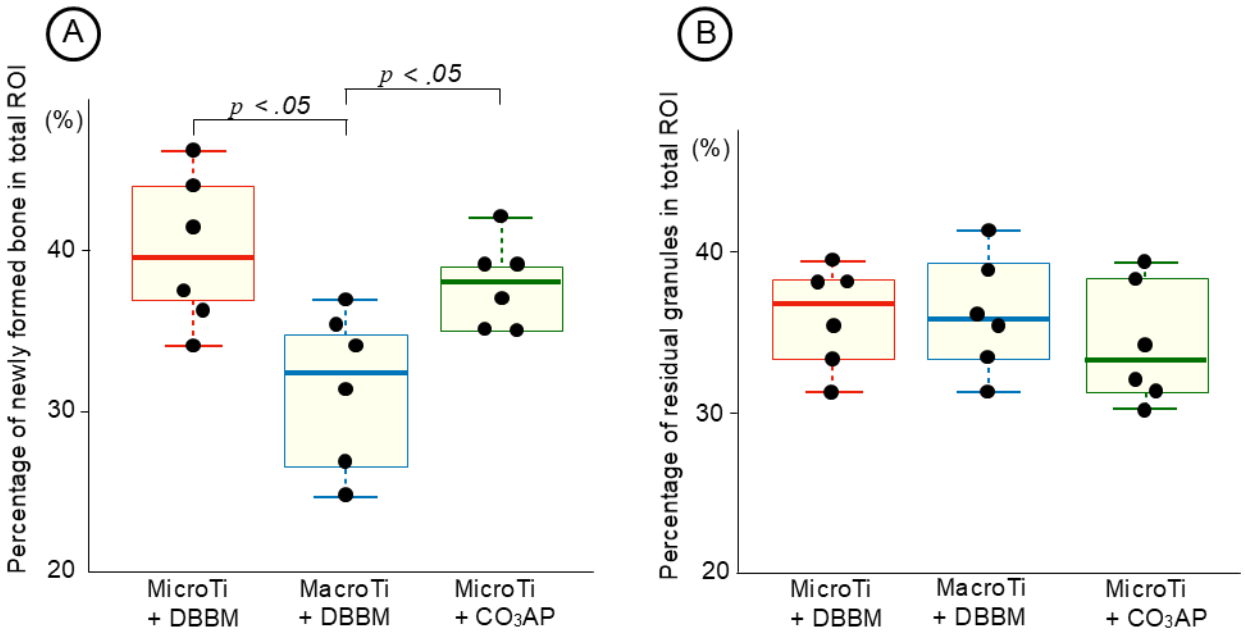

Fig. 7 Histomorphometric measurements of each parameter after 12 weeks of healing are represented as box plots. Percentage of newly formed bone in total region of interest (ROI) (%) (A); Percentage of residual granules in total ROI (%) (B). The points show the data for all specimens. The median, percentiles, and maximum and minimum values of each group are displayed.

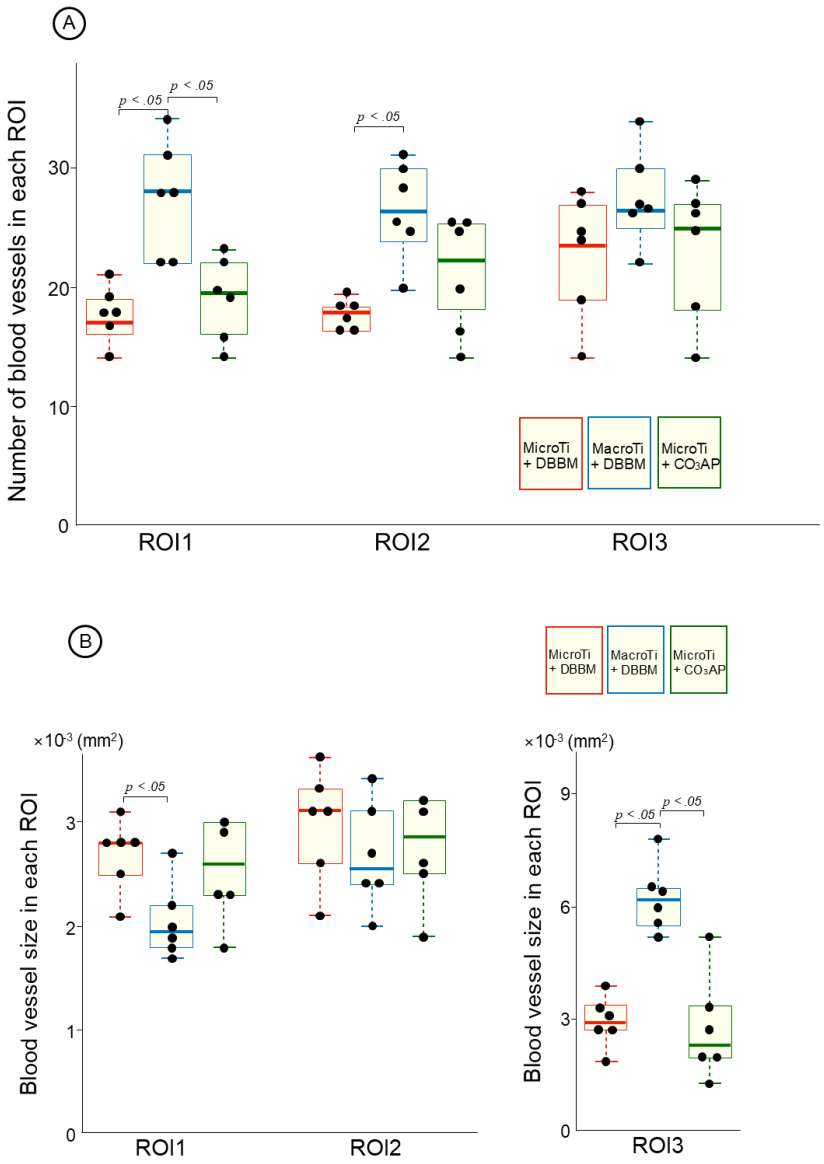

Fig. 8 Histomorphometric measurements of angiogenetic parameters after 12 weeks of healing are represented as box plots. Number of blood vessels in each ROI (A); Blood vessel size in each ROI (mm^2) (B). The median, percentiles, and maximum and minimum values of each group are displayed.

Table

Table 1 Volumetric measurements from micro-computed tomography analysis (mm^3)

Bone Volume (mm^3)	4 weeks		8 weeks		12 weeks	
MicroTi + DBBM	0.64	(2.09)	1.17	(1.72)	1.81	(1.50)
MacroTi + DBBM	3.17	(0.54)	3.42	(0.73)	3.65	(0.28)
MicroTi + CO_3AP	2.04	(0.92)	2.08	(1.46)	2.54	(1.40)

Values are represented as mean (SD).

There are no significant differences between any groups.

MacroTi, macroporous titanium lid; DBBM, deproteinized bovine bone mineral; CO_3AP, carbonate apatite; MicroTi, microporous titanium lid.